Fault Diagnosis in Industrial Induction Machines Through Discrete Wavelet Transform

Ahcène Bouzida, Omar Touhami, Rachid Ibtiouen, Adel Belouchrani, Maurice Fadel, A. Rezzoug

Fault Diagnosis in Industrial Induction Machines Through Discrete Wavelet Transform

Ahcène Bouzida, Omar Touhami, Rachid Ibtiouen, Adel Belouchrani, Maurice Fadel, and A. Rezzoug

***Abstract*—This paper deals with fault diagnosis of induction machines based on the discrete wavelet transform. By using the wavelet decomposition, the information on the health of a system can be extracted from a signal over a wide range of frequencies. This analysis is performed in both time and frequency domains. The Daubechies wavelet is selected for the analysis of the stator current. Wavelet components appear to be useful for detecting different electrical faults. In this paper, we will study the problem of broken rotor bars, end-ring segment, and loss of stator phase during operation.**

***Index Terms*—Broken rotor bars, data-dependent selection (DDS) and data-independent selection (DIS) of the decomposition level, fault diagnosis, induction machines (IMs), motor-current signature analysis (MCSA), wavelet transform.**

NOMENCLATURE

$\psi(n)$	Bandpass filter.
$\varphi(n)$	Low-pass filter.
A_j	Approximation signal.
$D_1\ D_2, \ldots, D_j$	Detail signals.
$W_f(t)$	Original signal.
$\hat{\psi}(\omega), \hat{\varphi}(\omega)$	Fourier transforms of $\psi(n)$ and $\varphi(n)$.
N_s	Samples.
$H(x)$	Entropy.
$x[n]$	Signal of length n.
j	Level of decomposition.
E_j	Energy eigenvalue.
T	Eigenvector.
P_n	Rated power.
V_s	Rated voltage.
I_s	Rated current.
N_n	Rated speed.
p	Pole-pair number.
m	Number of phases.
f	Supply frequency.
$\cos\Phi$	Power factor.

Manuscript received September 23, 2009; revised March 18, 2010 and June 14, 2010; accepted October 7, 2010. Date of publication November 29, 2010; date of current version August 12, 2011. This work was supported in part by the Laboratoire de Recherche en Electrotechnique, Ecole Nationale Polytechnique, Algiers, in part by the Laboratoire Plasma et Conversion d'Energie (LAPLACE), École Nationale Supérieure d'électronique, d'Électrotechnique, d' Informatique, d'Hydraulique et des Télécommunications (ENSEEIHT), Toulouse, Comité Mixte d'Evaluation et de Prospective (CMEP)-Tassili, under Code 05 MDU 662, and in part by the Algerian Ministry of High Education.

A. Bouzida, O. Touhami, R. Ibtiouen, and A. Belouchrani are with the Ecole Nationale Polytechnique, Algiers 16200, Algérie (e-mail: ahcene2035@hotmail.com; omar.touhami@enp.edu.dz; rachid.ibtiouen@enp.edu.dz; adel.belouchrani@enp.edu.dz).

M. Fadel is with the Laboratoire Plasma et Conversion d'Energie 2, 31071 Cedex 7, France (e-mail: fadel@laplace.univ-tlse.fr).

A. Rezzoug is with the Ecole nationale Supérieure d'Électricité et de Mécanique, 54516 Vandoeuvre lès Nancy, France (e-mail: rezzoug@green.uhp-nancy.fr).

Color versions of one or more of the figures in this paper are available online at http://ieeexplore.ieee.org.

Digital Object Identifier 10.1109/TIE.2010.2095391

I. INTRODUCTION

SQUIRREL-CAGE induction machines (IMs) are dedicated for electric drives and play an important role in manufacturing environments. Therefore, this type of machines is generally considered, and several diagnostic procedures are proposed in the literature [1]–[10].

Specific uses of IMs do not tolerate inopportune breakdowns. These breakdowns can be due to the machine and can be of mechanical origin (rotor eccentricity, coupling defect, bearing defects, etc.) or of electric and magnetic origin (short circuit in stator windings, broken bars, broken end ring, or broken teeth). The imperfections can also be due to other elements of the drive, such as defects in the power supply, load, or mechanical reducers.

Motor-current signature analysis (MCSA) is one of the most widely used techniques in fault-detection analysis of IMs. MCSA focuses its efforts on the spectral analysis of the stator current, and it has been successfully used in the detection of broken rotor bars, bearing damage, and dynamic eccentricity caused by a variable air gap due to a bent shaft or thermal bow. The procedure consists of evaluating the relative amplitude of current harmonics that appear due to this defect.

Wavelet transform is an analysis method for time-varying or nonstationary signals and uses a description of spectral decomposition via the scaling concept. Wavelet theory provides a unified framework for a number of techniques which have been developed for various signal-processing applications [11]–[19]. One of its feature is multiresolution signal analysis with a vigorous function of both time and frequency localization. This method is effective for stationary as well as nonstationary signal processing. References [20] and [21] describe the pyramidal algorithm based on convolutions with quadrature-mirror filters, which is a fast method similar to the fast Fourier transform, for signal decomposition and reconstruction. It can be interpreted as a decomposition of the original signal in an orthonormal wavelet basis or as a decomposition of the signal in a set of independent frequency bands. This independence is due to the orthogonality of the wavelet functions [22].

In this paper, a method for the diagnosis of broken rotor bars, broken end ring, and the opening of stator phase during

operation is described. The approach is also compared with the well-known Fourier method for the analysis of the stator current in steady-state operation. Several experiments are developed for different fault cases and operating conditions, such as healthy rotor, one broken bar, two broken bars, and one end-ring portion broken. In this paper, two different methods [data-dependent selection (DDS) and data-independent selection (DIS)] have been used to select the decomposition levels necessary for information extractions corresponding to defects due to stator currents. The experiments have been particularly done at a laboratory on four constructed machines for diagnosis purposes. A *data acquisition system* (DAS) and current and voltage sensors are also used for the purpose of the experiment.

The use of wavelet signals (approximation and high-order details) resulting from discrete wavelet transform *(DWT)* constitutes an interesting advantage because these signals act as filters, according to Mallat's algorithm, allowing automatic extraction of the time evolution of the low-frequency components that are present in the signal during transient operation.

II. Description of the Wavelet Method

The wavelet method requires the use of time–frequency basis functions with different time supports to analyze signal structures of different sizes. The wavelet transform, an extension of the short-time Fourier transform, projects the original signal down into wavelet basis functions and provides a mapping from the time domain to the time-scale plane.

A wavelet is a function belonging to $L^2(R)$ with a zero average. It is normalized and centered on the neighborhood of $t = 0$. A time–frequency atom family is obtained by scaling a bandpass filter ψ by s and translating it by u. $L^2(R)$ represents the space vector of measurable square-integrable functions on the real line R with $\|\psi\| = 1$

$$\int_{-\infty}^{+\infty} \psi(t)dt = 0 \tag{1}$$

$$\psi_{u,s}(t) = \frac{1}{\sqrt{s}}\psi\left(\frac{t-u}{s}\right). \tag{2}$$

The wavelet transform of a function f at the scale s and position u is computed by correlating f with a wavelet atom

$$W_f(u,s) = \int_{-\infty}^{+\infty} f(t)\frac{1}{\sqrt{s}}\psi\cdot\left(\frac{t-u}{s}\right)dt. \tag{3}$$

A real wavelet transform is complete and conserves energy as long as it satisfies a weak admissibility condition

$$\int_{0}^{+\infty} \frac{|\psi(\omega)|^2}{|\omega|}d\omega = \int_{-\infty}^{0} \frac{|\psi(\omega)|^2}{|\omega|}d\omega = C_\psi < +\infty. \tag{4}$$

When $W_f(u,s)$ is known only for $s < s_0$, we need to recover f, a complement of information corresponding to $W_f(u,s)$, for $s > s_0$. This is obtained by introducing a scaling function φ that is a wavelet aggregate at scales larger than one. In the sequel, we design by $\hat{\psi}(\omega)$ and $\hat{\varphi}(\omega)$ the Fourier transforms of $\psi(n)$ and $\varphi(n)$, respectively.

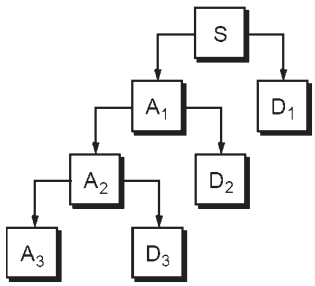

Fig. 1. Tree decomposition of the signal S.

The DWT results from the continuous version. Unlike the latter, the DWT uses a discrete scale factor and a translation. One calls DWT dyadic into any base of wavelet working with a scale factor $u = 2^j$.

The discrete version of wavelet transform DW consists of sampling neither the signal nor the transform but sampling the scaling and shifted parameters [25]–[27]. This results in high frequency resolution at low frequencies and high time resolution at high frequencies, removing the redundant information. Taking positive frequency into account, $\hat{\varphi}(\omega)$ has information in [0, π], and $\hat{\psi}(\omega)$ has information in $[\pi, 2\pi]$. Therefore, they both have complete signal information without any redundancy. Functions $h(n)$ and $g(n)$ can be obtained by the inner product of $\psi(t)$ and $\varphi(t)$. Decomposition of the signal in [0, π] gives [11]

$$\begin{aligned} h(n) &= \left\langle 2^{-l}\varphi(2^{-l}t)\varphi(t-n)\right\rangle \\ g(n) &= \left\langle 2^{-j}\psi(2^{-j}t)\varphi(t-n)\right\rangle, \qquad j = 0,1,\ldots. \end{aligned} \tag{5}$$

Wavelet decomposition does not involve the signal in $[\pi, 2\pi]$. In order to decompose the signal in the whole frequency band, wavelet packets can be used. After decomposing by l times, we get 2^l frequency bands each with the same bandwidth, i.e.,

$$\left[\frac{(i-l)f_n}{2}, \frac{if_n}{n}\right], \qquad i = 1,2,\ldots,2^l \tag{6}$$

where f_n is the Nyquist frequency in the ith-frequency band. Wavelet packets decompose the signal into one low-pass filter $h(n)$ and $(2^l - 1)$ bandpass filters $g(n)$ and provide diagnosis information in two frequency bands. A_j is the low-frequency approximation, and D_j is the high-frequency detail signal, both at resolution j

$$\begin{aligned} A_j(n) &= \sum_k h(k-2n)A_{j-1} \\ D_j(n) &= \sum_k g(k-2n)A_{j-1}, \qquad n = 1,2,3\ldots \end{aligned} \tag{7}$$

where $A_0(k)$ is the original signal. After decomposing the signal, we obtain one approximation signal A_j and $D_1,\ D_2,\ldots,D_j$ detail signals (see Fig. 1).

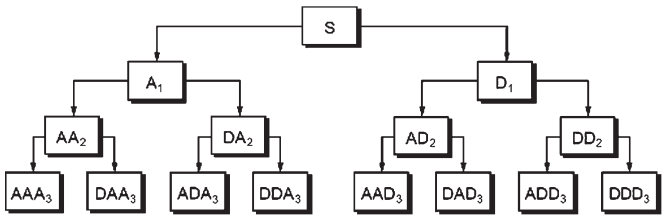

Fig. 2. Decomposition of the signal S in the wavelet packet.

The wavelet-packet method is a generalization of wavelet decomposition that offers a richer range of possibilities for signal analysis (see Fig. 2). In wavelet analysis, a signal is split into an approximation and a detail. Then, the approximation is itself split into a second-level approximation and detail, and the process is repeated [24] until the targeted results are obtained. For n-level decomposition, there are $n+1$ possible ways to decompose or encode the signal

$$W_{2n}(t) = \sqrt{2}\sum_k h(k)W_n(2t-k)$$

$$W_{2n+1}(t) = \sqrt{2}\sum_k g(k)W_n(2t-k) \tag{8}$$

where $W_f(t)$ is the original signal. By comparing (8) with (7), we can find that not only A_j in (7) is decomposed but D_j in (8) is also decomposed.

Wavelets and wavelet packets decompose the original signal, which is nonstationary or stationary, into independent frequency bands with multiresolution [24].

III. Experimental Tests

A. MCSA

Four rotors have been used in the tests, as shown in Fig. 3. In order to obtain correct resolution for the wavelet analysis, it is important to choose correctly the acquisition parameters, i.e., the sampling frequency and number of samples. Some constraints are also taken into consideration:

1) analyzed signal bandwidth;
2) wavelet decomposition spectral bands;
3) frequency resolution;
4) appropriate number of decomposition.

For an IM, significant information in stator current signal is concentrated in the 0–400-Hz band. Applying the Shannon's theorem yields a minimum sampling frequency fs of 800 Hz.

The minimum resolution needed to get a good result is 0.5 Hz. Equation (9) defines the number of samples N_s needed for a given resolution R [20]–[22]

$$N_s = \frac{f_s}{R}. \tag{9}$$

In our case, we have chosen a sampling frequency $fs = 10$ kHz. Hence, $N_s = 100\,000$ samples are acquired for $R = 0.1$ Hz. The analyzed frequencies vary from 0 to 5 kHz with a resolution of 0.1 Hz.

Fig. 4 shows the experimental setup where different 4-kW IMs are used to test the performance of the proposed methodology in identifying different faults treated in this paper. This system can be used to sample two line currents I_a and I_b, three line voltages V_a, V_b, and V_c, and a speed signal. The stator

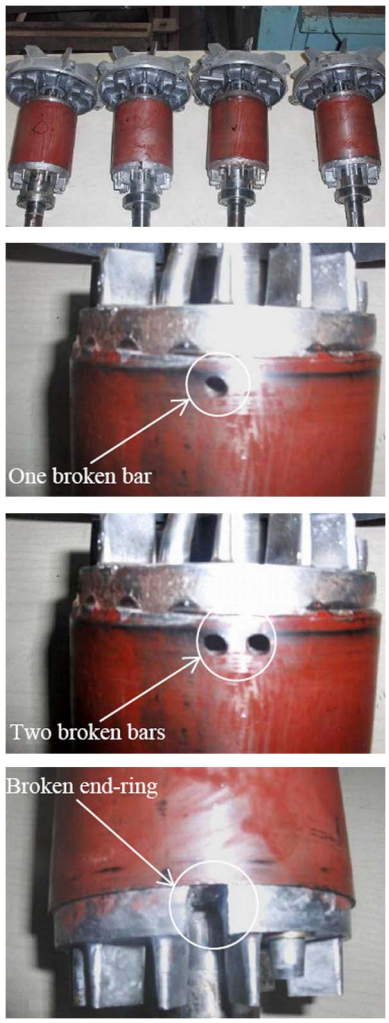

Fig. 3. Four rotors under tests.

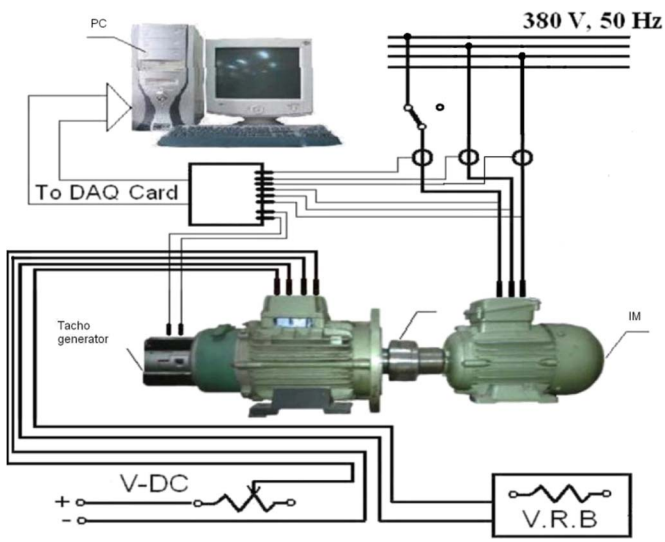

Fig. 4. Experimental setup.

TABLE I
ENTROPY ON LEVELS

Levels	Healthy machine 1	Faulty machine 2	Faulty machine 3	Faulty machine 4
j=1	0.0010	0.0008	0.0011	0.0006
j=2	0.0042	0.0039	0.0089	0.0026
j=3	0.0582	0.0977	0.0313	0.0771
j=4	0.143	0.1129	0.0211	0.0534
j=5	0.0045	-0.062	0.0701	0.1651
j=6	0.0020	0.0230	0.0179	0.0770

windings are star connected. The main parts of the experimental setup are as follows:

1) three-phase 4-kW IM;
2) dc generator coupled to the IM to provide load;
3) tachogenerator coupled to the shaft of the generator as angular-speed sensor to measure and record the time variation of the speed;
4) mechanical coupling between the IM and the dc generator;
5) single-phase changeover switch for opening the stator phase;
6) PC equipped with a data acquisition card of PCI-IOTEQ type for sampling the electrical data at a certain adjustable frequency and storing them in the memory.

The tested machines have two pole pairs $(p = 2)$ and 28 bars and receive a power supply of 220-V ac at 50 Hz. For the rotor faults, the machines are tested at 75% of rated load and no load for the loss of stator phase test.

We have experimented two different methods for the selection of wavelet decomposition level, namely, the approach presented in [26], referred herein as DDS, and the approach of reference referred herein as DIS.

B. DDS of the Decomposition Level

The DDS approach is based on the decomposition of entropy data at each level, as follows.

1) The entropy-based criterion is used to find the desired levels of resolution. The entropy $H(x)$ of a signal $x[n]$ of length N is defined by

$$H(x) = -\sum_{n=0}^{N-1} |x(n)|^2 \log |x(n)|^2 . \tag{10}$$

2) To determine the optimal number of levels of resolution, the entropy is evaluated at each level where there is a new level j such that

$$H(x)_j \geq H(x)_{j-1}. \tag{11}$$

The entropy of the first-level high-frequency details is found to be lower than that of its two children in all situations. As a result, according to (10), decomposition up to the first level is sufficient to represent the discrete signals. Table I presents the entropy on levels.

TABLE II
FREQUENCY BANDS OBTAINED BY DECOMPOSITION IN MULTILEVELS

Level	Approximations		Details	
J = 1	A1	0 - 5000	D1	5000 - 10000
J = 2	A2	0 - 2500	D2	2500 - 5000
J = 3	A3	0 - 1250	D3	1250 - 2500
J = 4	A4	0 - 625	D4	625 - 1250
J = 5	A5	0 - 312.50	D5	312.5 - 625
J = 6	A6	0 - 156.25	D6	156.25 - 312.5
J = 7	A7	0 - 78.125	D7	78.125 - 156.25
J = 8	A8	0 - 39.0625	D8	39.0625 - 78.125
J = 9	A9	0 - 19.5313	D9	19.53 - 39.0625

C. DIS of the Decomposition Level

The DIS approach is based on the following.

1) A suitable number of decomposition levels (n_{Ls}) depend on the sampling frequency fs of the signal being analyzed. For each one of the proposed approaches [23], [25], [26], it has to be chosen in order to allow the high-level signals (approximation and details) to cover all the range of frequencies along which the sideband is localized.
2) The minimum number of decomposition levels that is necessary for obtaining an approximation signal (A_{nf}) so that the upper limit of its associated frequency band is under the fundamental frequency [17] is described by the following condition:

$$2^{-(n_{Ls}+1)} f_s < f. \tag{12}$$

From this condition, the decomposition level of the approximation signal, which includes the left sideband harmonic, is the integer n_{Ls} given by

$$n_{Ls} = \text{int}\left(\frac{\log(fs/f)}{\log(2)}\right). \tag{13}$$

For this approach, further decomposition of this signal has to be done so that the frequency band $[0 - f]$ will be decomposed in more bands. Usually, two additional decomposition levels (i.e., $n_{Ls} + 2$) would be adequate for the analysis [17]

$$\begin{aligned} n_{Ls} + 2 &= \text{int}\left(\frac{\log(10\,000/50)}{\log(2)}\right) + 2 \\ &= \text{int}(7.64) + 2 = 9 \text{ levels}. \end{aligned} \tag{14}$$

For the healthy IM, the selected level from the DDS and DIS approaches are quite the same, while for the machines with defects, the DDS approach gives a lower level than the DIS. This is clear from the obtained results (see Figs. 9–11) that the lower level provided by the DDS does not get the true results because it requires more levels for defect detection. It is recommended then to choose the second method (DIS). For this case, the wavelet decomposition tree is shown in Table II.

One seeks information characterizing the defect for a frequency ranging between 0 and 100 Hz. For the DDS method, the level of decomposition ($J = 4$ and $J = 5$) gives

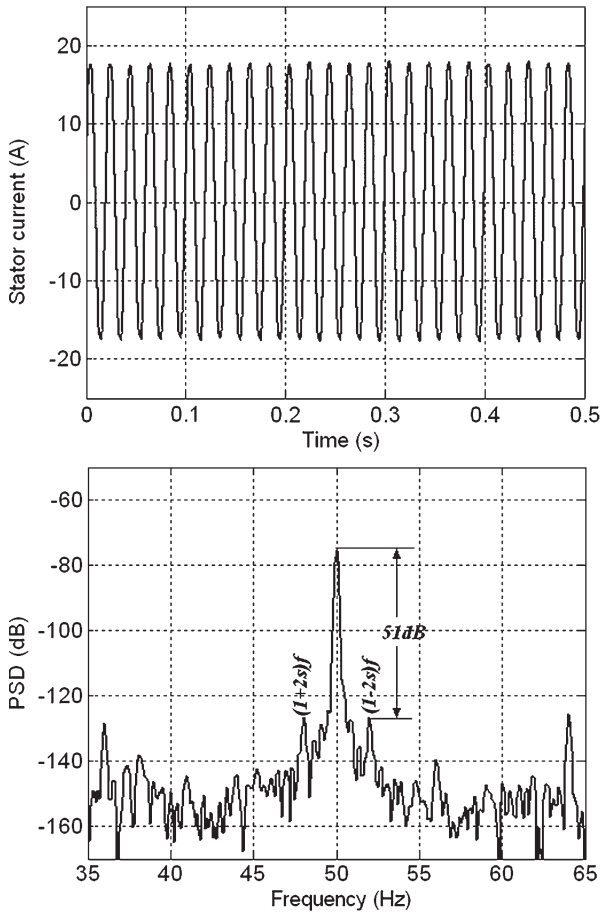

Fig. 5. Stator current of a healthy IM and its normalized PSD.

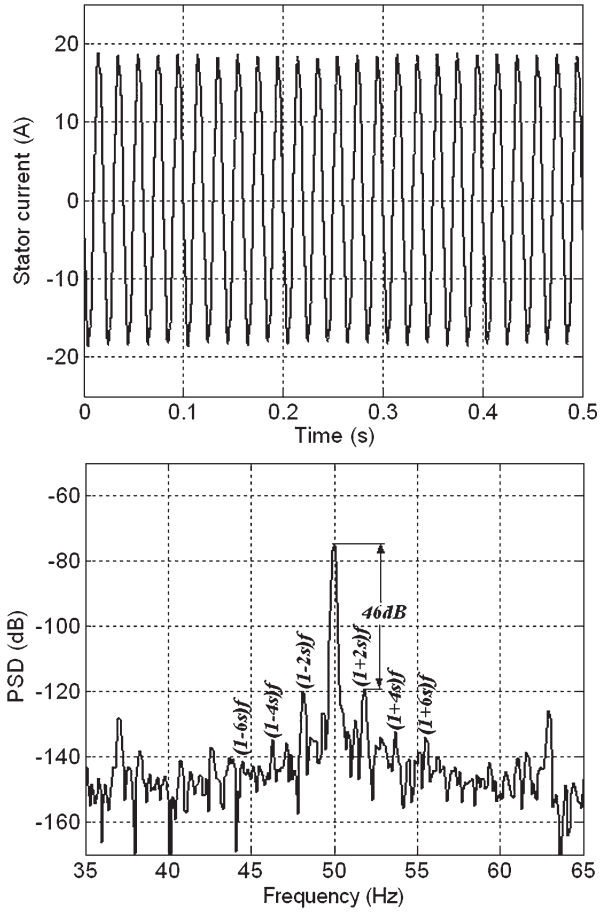

Fig. 6. Stator current of an IM with a broken rotor bar and its normalized PSD.

approximations and details ($A5,\ D5$) in a waveband between 0 and 625 Hz (see Table I).

On the other hand, for the second method (DIS), the level of decomposition ($J = 9$) gives approximations and details ($A9,\ D9$) in a waveband ranging between 0 and 39.6 Hz (see Table II). Thus, the choice of the method (DIS) becomes commonplace.

Several types of mother wavelets exist (Daubechies, coiflet, simlet, biorthogonal, etc.) and have different properties [17]. However, some authors showed that all these types of mother wavelets gave similar results. Due to the well-known properties of the orthogonal Daubechies family, we chose to use a mother wavelet from this family.

The multilevel decomposition of the stator current was then performed using Daubechies wavelet; the suitable level of decomposition is calculated according to (13). When the defect of the rotor bars, end-ring portion, and short-circuit on the stator windings of the induction motor appear, the defect information in the stator current is included in each frequency band determined by the decomposition in the wavelet or in wavelet packet. By calculating the energy associated to each level or with each node of decomposition, one can build a very effective diagnosis tool. The energy eigenvalue for each frequency band is defined by [20]–[22]

$$E_j = \sum_{k=1}^{k=n} |D_{j,k}(n)|^2 . \tag{15}$$

Based on the energy eigenvalue, the eigenvector is set up as

$$T = \left[\frac{E_0}{E}, \frac{E_1}{E}, \frac{E_2}{E}, \ldots\ldots, \frac{E_{2^l-1}}{E} \right] \tag{16}$$

where $j = 1, 2, \ldots, 2^l - 1$; D_j is the amplitude in each discrete point of the wavelet coefficient of the signal in the corresponding frequency band, with $E = \sum_{j=0}^{2^m-1} |E_j|^2$.

The eigenvalue T contains information on the signal of the stator current for a motor behavior. In addition, the amplitudes of the deviation of some eigenvalues indicate the severity of the defect, which makes T a good candidate for diagnosing broken bars of the rotor and/or defect of the end-ring portion.

The power spectral density (PSD) of the stator current clearly shows the increase of the amplitudes in relation with the defects of the rotor $(1 \pm 2s)f$. Figs. 5–8 show the PSD of the stator current in the four cases.

D. DWT Applied to the Stator Current

The "Daubechies wavelets" of different order are used to decompose the stator current of each machine. Fig. 9 shows the detail and approximation signals ($D9$, $D8$, $D7$, and $A6$) obtained by $db44$. The calculation of the energy eigenvector T indicates the variation of this energy in the four machines, as shown in Figs. 10–12.

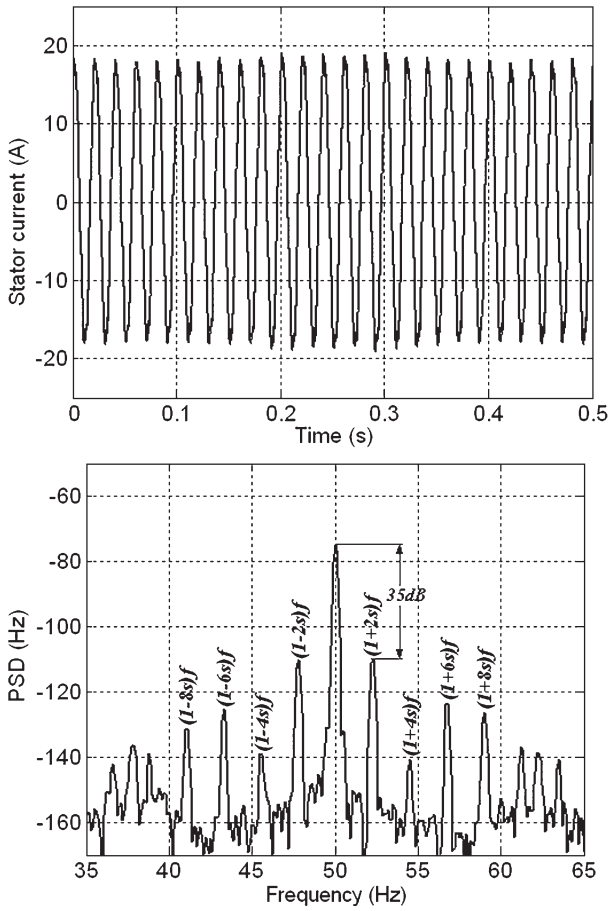

Fig. 7. Stator current of an IM with two broken rotor bars and its normalized PSD.

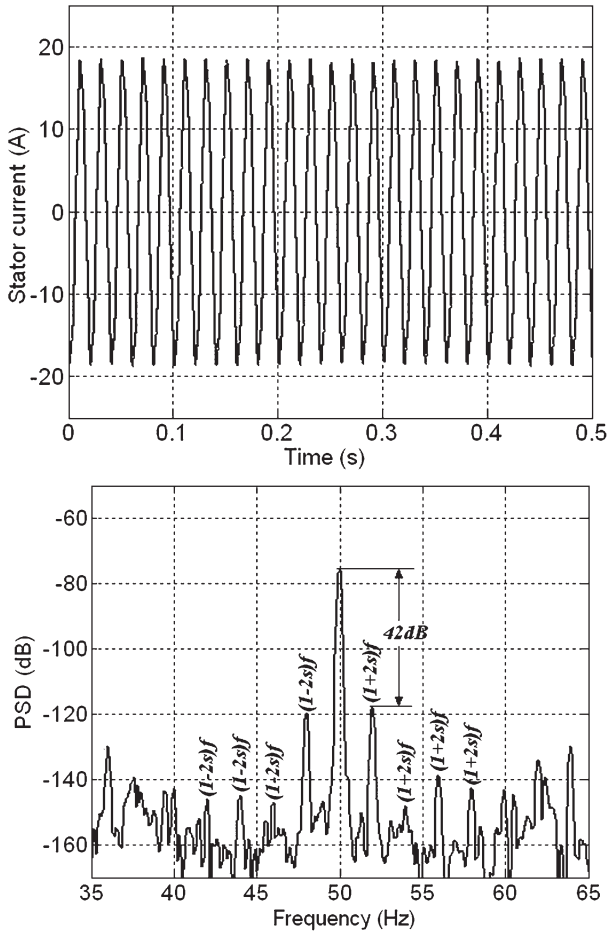

Fig. 8. Stator current of an IM with a broken end-ring portion and its normalized PSD.

In Fig. 9, the evolution in the observed frequency bands of the relative signal to the rotor defect can be analyzed using coefficients $D9$ and $D8$ to $D7$ or using only coefficient $A6$ that gives all the information in the frequency band [0–156.25 Hz]. While analyzing the effect of the rotor defect in the bands of the frequencies of interest, one can see that the energy depends on the type of defect. For all the studied machines, the difference between the healthy rotor and the deficient rotors is clearly shown in Fig. 10.

Figs. 11 and 12 clearly show the variation of the energy eigenvalue. One can observe that the energy stored in band 7 depends on the degree of the default. Obviously, the energy in level 7 represents the number of broken bars and the broken end-ring portion of the squirrel-cage rotor. Figs. 10–12 show that the choice of the mother wavelet and its order has a great importance in differentiating the energies because, when the order of the mother wavelet is increased, the difference between the energy eigenvalues becomes clearer.

The band of detection of broken rotor bars cannot be influenced by mechanical vibrations and load effect because the frequencies accompanying the mechanical problem are very far from the band of detection, which is located in [39.06–78.12] Hz. The broken bar and end-ring portion induce supplementary frequencies near the fundamental component which are described by $(1 \pm 2s)f$. These frequencies are influenced only by the operating frequency f and the slip s; however, this method is not dependent on the motor power, but we must choose the appropriate band and the decomposition of the stator current.

E. Application to Residual Stator Current

The extraction of the fundamental component leads to a signal full of information. Indeed the elimination of the dominant component in the stator current contributes to amplify the components due to defects. For this reason, we make the stator current go through a bandpass filter to eliminate the 50-Hz frequency. This method produces attenuation in some components.

Figs. 13 and 14 show the residual stator current and their normalized PSD.

Looking at Figs. 15 and 16, one can note that the extraction of the fundamental has a very significant effect on the diagnosis of defaults. This effect is interpreted by the increase in the amplitudes of the signals in bands $D7$ and $A6$, in the case of defect compared with the healthy case. The effect of the extraction also leads to a differentiation in the energies stored in the levels between the various machines, not only in level 7 but also in levels 1, 2, 3, 4, 5, 6, and 7. According to the previous results, one can also note that the effect of the broken rotor bar is similar to that of a broken end-ring portion.

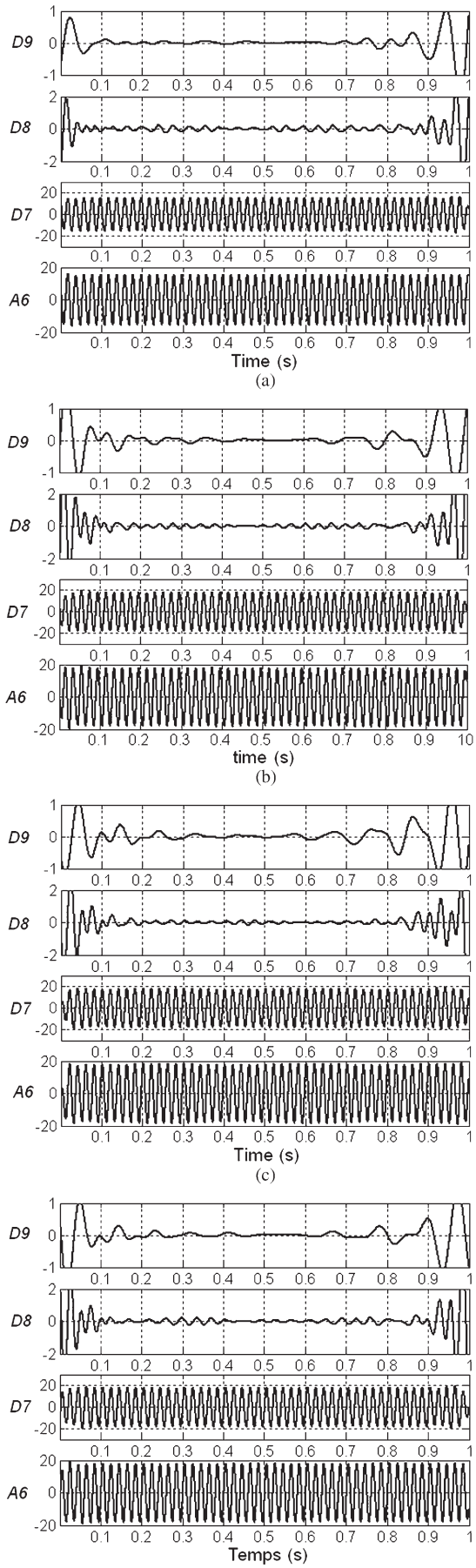

Fig. 9. Details and approximation for (a) healthy, (b) one broken bar, (c) two broken bars, and (d) broken end ring.

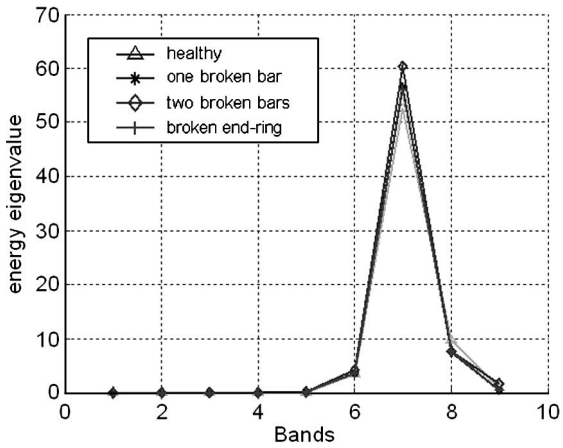

Fig. 10. Eigenvector analysis results obtained from *db*6.

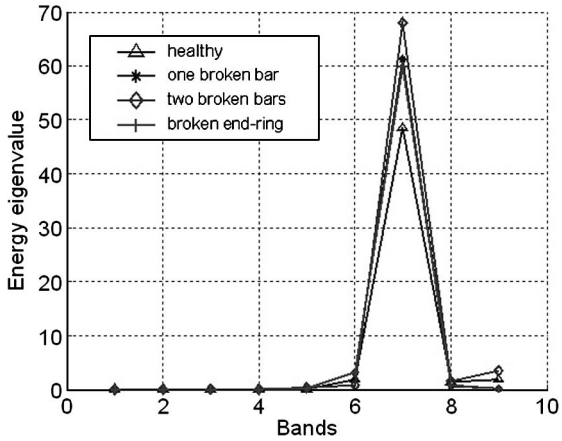

Fig. 11. Eigenvector analysis obtained from *db*24.

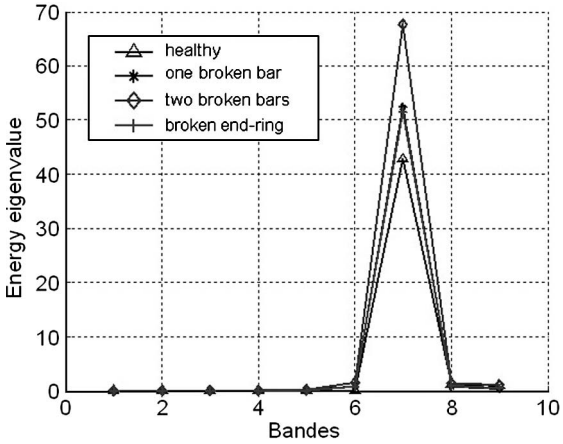

Fig. 12. Eigenvector analysis results obtained from *db*44.

F. Nonstationary Detection

The opening of stator phase "*b*" during running is one of the defects that can appear in the IM. This defect is accompanied by unbalance and vibrations capable of causing a real danger to the coils of the two other phases. Figs. 17–19 show the stator currents of healthy IM, including the period of opening of phase *b* during operation at no-load tests.

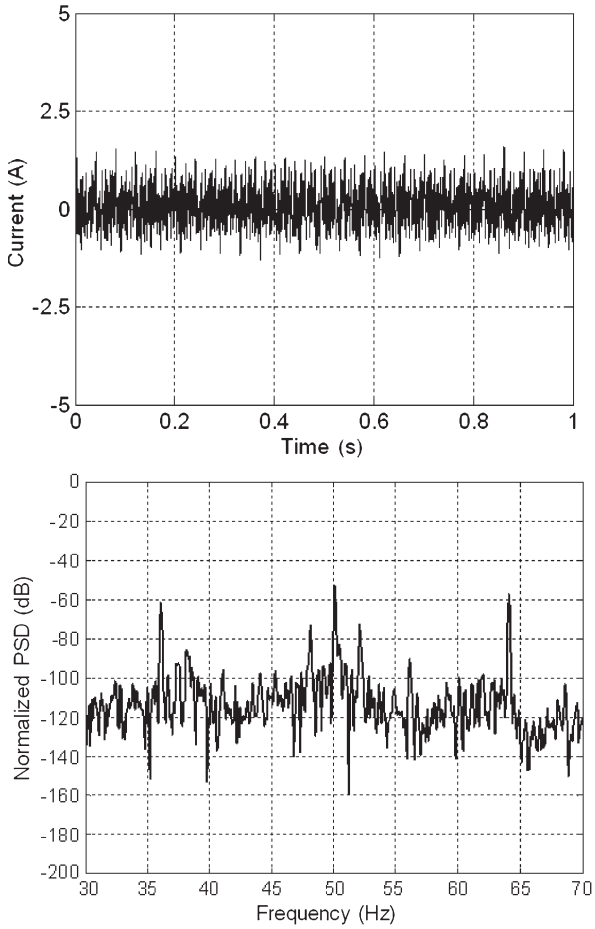

Fig. 13. Residual stator current of healthy machine and its normalized PSD.

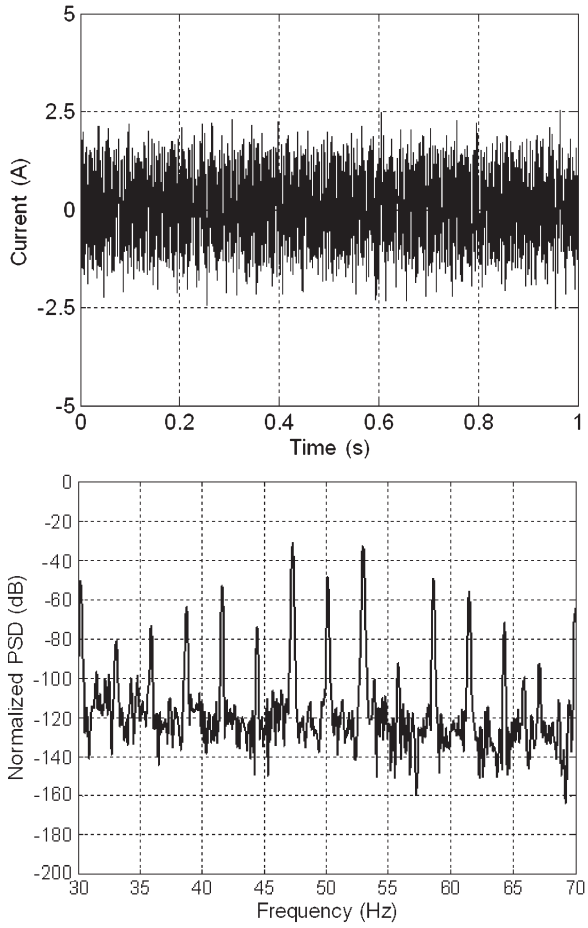

Fig. 14. Residual stator current of machine with two broken bars and its normalized PSD.

To analyze the nonstationarity which occurred in the stator current and voltage at the moment of opening a stator phase, we carried out the decomposition of the two signals in multilevel and wavelet packet by using the $db44$ mother wavelet. Figs. 20–22 show the obtained signals of the details and approximation.

The opening of a stator phase is well represented by the signature of the motor current, and it is largely sufficient to identify this defect from Figs. 17 and 18.

For the voltage, no defect appears because the voltage is imposed by the network. However, by using the decomposition technique of the wavelet packets, one can rigorously show the opening moment of a stator phase, as shown in Fig. 22.

It can be noted that the use of the wavelet technique enables us to extract and to locate the point of nonstationarity in the nonstationary signals [28]–[31]. The nonstationarity induced by the opening of stator phase is extracted in the two details of $D9$ and $D8$. The decomposition in the wavelet packets confirms the results obtained by the decomposition in multilevel; nonstationarity is detected in all the frequency bands leading to an increase in the amplitude of the current after the opening of a phase. The wavelets are inherently suited for nonstationary signal analysis since it neither requires the use of windowing nor is dependent on any assumption on local stationarity [31], [32]. One concludes that the defect of the opening of a phase generates an abrupt variation of frequency at the time of the opening and an increase in amplitude of the stator currents. All the other faults which can produce a nonstationarity in the machine, like short circuit, fluctuation of load, ...) could be detected by the wavelet decomposition.

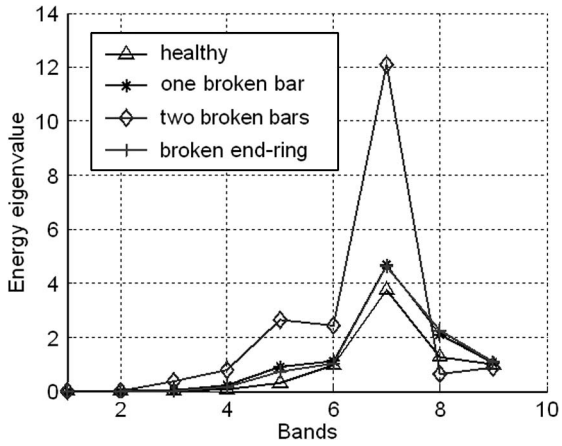

Fig. 15. Eigenvector analysis results obtained from $db24$.

IV. Conclusion

Signal decomposition via wavelet transform and wavelet packets provides a good approach of multiresolution analysis.

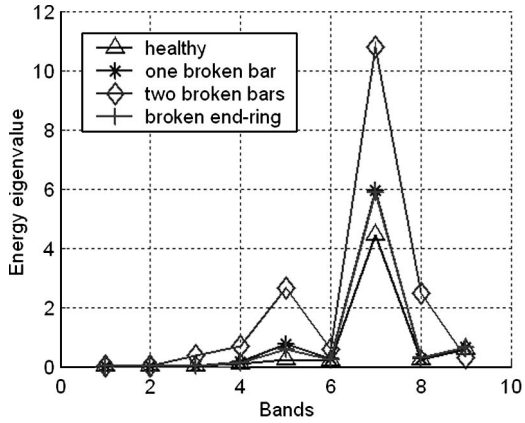

Fig. 16. Eigenvector analysis results obtained from $db6$.

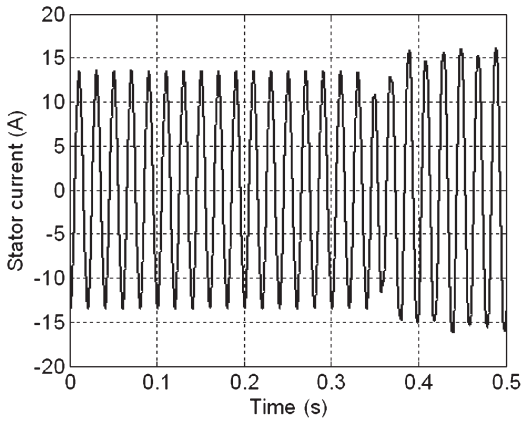

Fig. 17. Stator current in phase "a" during the opening of phase b.

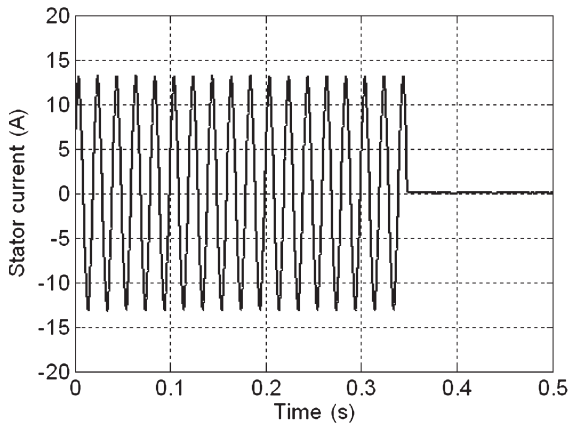

Fig. 18. Stator current during the opening of the disconnected phase.

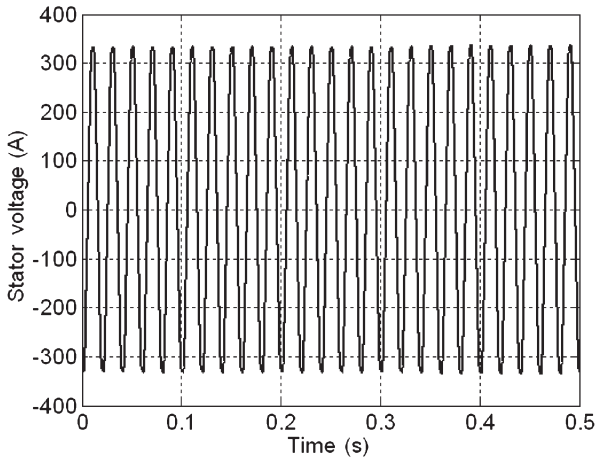

Fig. 19. Stator voltage U_{ca} during the opening of phase b.

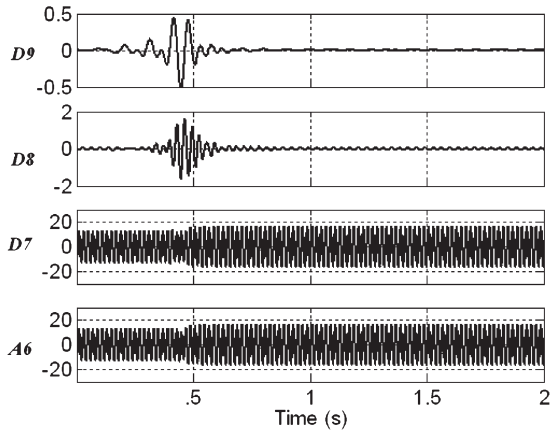

Fig. 20. Details and approximation obtained by decomposition in the multilevel stator current during opening.

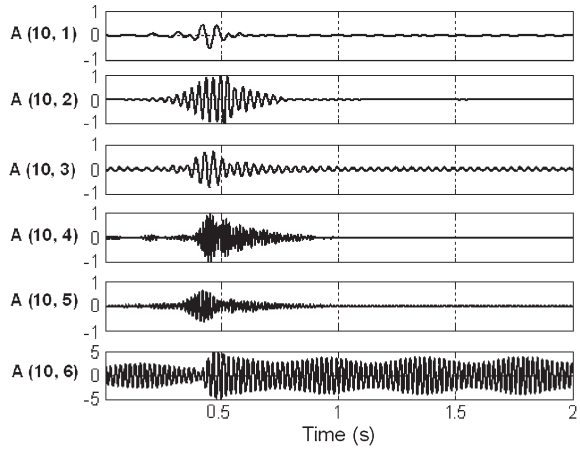

Fig. 21. Details and approximation obtained by decomposition in the wavelet packet of the stator current during opening.

The decomposed signals are independent due to the orthogonality of the wavelet function. There is no redundant information in the decomposed frequency bands.

Based on the information from a set of independent frequency bands, mechanical-condition monitoring and fault diagnosis can be effectively performed.

This paper has shown a new approach in detection of broken rotor bars and the nonstationarity in induction motor having only stator currents as input. The detection is based on the discrete wavelet decomposition method. The results show the effectiveness of the proposed method for this kind of fault.

MCSA is a good method for analyzing motor faults over constant load torque. However, in the case of nonconstant

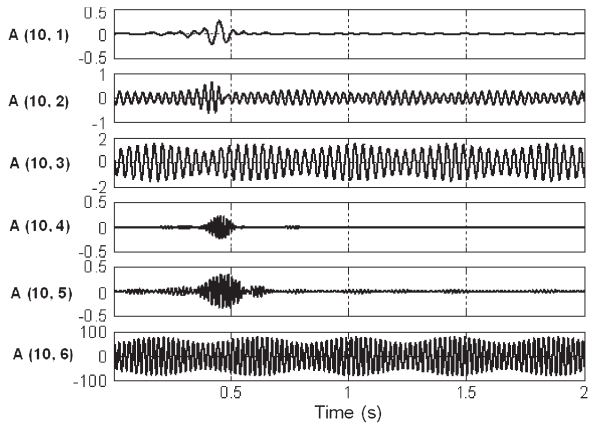

Fig. 22. Details and approximation obtained by decomposition in the wavelet packet of the stator voltage during opening.

load torque or nonstationary signals, the use of the wavelet decomposition is required.

APPENDIX

The name plate data of the squirrel cage IM are as follows:

$$P = 4\,\text{kW}; \quad V_s = 220/380\ \text{V}\ (\Delta/\text{Y});$$
$$I_s = 15.2/8.8\ \text{A}; \quad N_n = 1435\ \text{r/min};$$
$$p = 2; \quad m = 3; \quad f = 50\ \text{Hz}; \quad \cos\Phi = 0.83.$$

REFERENCES

[1] M. E. H. Benbouzid, "A review of induction motors signature analysis as a medium for faults detection," *IEEE Trans. Ind. Electron.*, vol. 47, no. 5, pp. 984–993, Oct. 2000.

[2] M. E. H. Benbouzid, M. Vieira, and C. Theys, "Induction motors faults detection and localisation using stator current advanced signal processing techniques," *IEEE Trans. Power Electron.*, vol. 14, no. 1, pp. 14–22, Jan. 1999.

[3] S. A. S. Al Kazzaz and G. K. Singh, "Experimental investigations on induction machine condition monitor and fault diagnosis using digital signal processing techniques," *Elect. Power Syst. Res.*, vol. 65, no. 3, pp. 197–221, Jun. 2003.

[4] H. Su and K. T. Chong, "Induction machine condition monitoring using neural network modeling," *IEEE Trans. Ind. Electron.*, vol. 54, no. 1, pp. 241–249, Feb. 2007.

[5] A. Lebaroud and G. Clerc, "Classification of induction machine faults by optimal time–frequency representations," *IEEE Trans. Ind. Electron.*, vol. 55, no. 12, pp. 4290–4298, Dec. 2008.

[6] M. Pineda-Sanchez, M. Riera-Guasp, J. A. Antonio-Daviu, J. Roger-Folch, J. Perez-Cruz, and R. Puche-Pandero, "Diagnosis of induction motor faults in the fractional Fourier domain," *IEEE Trans. Instrum. Meas.*, vol. 59, no. 8, pp. 2065–2075, Aug. 2010.

[7] B. Akin, U. Orguner, H. A. Toliyat, and M. Rayner, "Low order PWM inverter harmonics contributions to the inverter-fed induction machine fault diagnosis," *IEEE Trans. Ind. Electron.*, vol. 55, no. 2, pp. 610–619, Feb. 2008.

[8] J. F. Martins, V. F. Pires, and A. J. Pires, "Unsupervised neural-network-based algorithm for an on-line diagnosis of three-phase induction motor stator fault," *IEEE Trans. Ind. Electron.*, vol. 54, no. 1, pp. 259–264, Feb. 2007.

[9] S. H. Kia, H. Henao, and G.-A. Capolino, "Diagnosis of broken bar fault in induction machine using discrete wavelet transform without slip estimation," *IEEE Trans. Ind. Appl.*, vol. 45, no. 4, pp. 1395–1404, Jul./Aug. 2009.

[10] M. E. H. Benbouzid and G. B. Kliman, "What stator current processing based technique to use for induction motor rotor faults diagnosis?" *IEEE Trans. Energy Convers.*, vol. 18, no. 2, pp. 238–244, Jun. 2003.

[11] T. Tarasiuk, "Hybrid wavelet-Fourier spectrum analysis," *IEEE Trans. Power Del.*, vol. 19, no. 3, pp. 957–964, Jul. 2004.

[12] J. A. Antonio-Daviu, M. Riera-Guasp, J. R. Floch, and M. P. M. Palomares, "Validation of a new method for the diagnosis of rotor bar failures via wavelet transform in industrial induction machines," *IEEE Trans. Ind. Appl.*, vol. 42, no. 4, pp. 990–996, Jul./Aug. 2006.

[13] J. Faiz, B. M. Ebrahimi, B. Asaie, R. Rajabioun, and H. A. Toliyat, "A criterion function for broken bar fault diagnosis in induction motor under load variation using wavelet transform," in *Proc. ICEMS*, 2007, pp. 1249–1254.

[14] M. A. S. K. Khan, T. S. Radwan, and M. A. Rahman, "Real-time implementation of wavelet packet transform-based diagnosis and protection of three-phase induction motors," *IEEE Trans. Energy Convers.*, vol. 22, no. 3, pp. 647–655, Sep. 2007.

[15] J. Cusidó, L. Romeral, J. A. Ortega, J. A. Rosero, and A. G. Espinosa, "Fault detection in induction machines using power spectral density in wavelet decomposition," *IEEE Trans. Ind. Electron.*, vol. 55, no. 2, pp. 633–643, Feb. 2008.

[16] A. Ordaz-Moreno, R. de Jesus Romero-Troncoso, J. A. Vite-Frias, J. R. Rivera-Gillen, and A. Garcia-Perez, "Automatic online diagnosis algorithm for broken-bar detection on induction motors based on discrete wavelet transform for FPGA implementation," *IEEE Trans. Ind. Electron.*, vol. 55, no. 5, pp. 2193–2202, May 2008.

[17] J. A. Daviu, M. Riera-Guasp, J. Roger-Folch, F. Martínez-Giménez, and A. Peris, "Application and optimization of the discrete wavelet transform for the detection of broken rotor bars in induction machines," *Appl. Comput. Harmon. Anal.*, vol. 21, no. 2, pp. 268–279, Sep. 2006.

[18] J. K. Zhang, T. N. Davidson, and K. M. Wong, "Efficient design of orthonormal wavelet bases for signal representation," *IEEE Trans. Signal Process.*, vol. 52, no. 7, pp. 1983–1996, Jul. 2004.

[19] S. H. Kia, H. Henao, and G.-A. Capolino, "Diagnosis of broken-bar fault in induction machines using discrete wavelet transform without slip estimation," *IEEE Trans. Ind. Appl.*, vol. 45, no. 4, pp. 1395–1404, Jul./Aug. 2009.

[20] Z. Cvetkovic and M. Vetterli, "Discrete-time wavelet extrema representation: Design and consistent reconstruction," *IEEE Trans. Signal Process.*, vol. 43, no. 3, pp. 681–693, Mar. 1995.

[21] F. Niu and J. Huang, "Rotor broken bars fault diagnosis for induction machines based on the wavelets ridge energy spectrum," in *Proc. 8th ICEMS*, 2005, vol. 3, pp. 2274–2277.

[22] T. W. S. Chow and S. Hai, "Induction machine fault diagnostic analysis with wavelet technique," *IEEE Trans. Ind. Electron.*, vol. 51, no. 3, pp. 558–565, Jun. 2004.

[23] O. A. Mohamed, N. Y. Abed, and S. C. Ganu, "Modelling and characterization of induction motor internal faults using finite element and discrete wavelet transform," *IEEE Trans. Magn.*, vol. 42, no. 10, pp. 3434–3436, Oct. 2006.

[24] S. Rajagopalan, J. M. Aller, J. A. Restrepo, T. G. Habetler, and R. G. Harley, "Analytic-wavelet-ridge-based detection of dynamic eccentricity in brushless direct current (BLDC) motors functioning under dynamic operating conditions," *IEEE Trans. Ind. Electron.*, vol. 54, no. 3, pp. 1410–1419, Jun. 2007.

[25] R. Supangat, N. Ertugrul, W. L. Soong, D. A. Gray, C. Hansen, and J. Grieger, "Detection of broken rotor bars in induction motor using starting-current analysis and effects of loading," *Proc. Inst. Elect. Eng.—Elect. Power Appl.*, vol. 153, no. 6, pp. 848–855, Nov. 2006.

[26] Z. Ye, B. Wu, and A. Sadeghian, "Current signature analysis of induction motor mechanical faults by wavelet packet decomposition," *IEEE Trans. Ind. Electron.*, vol. 50, no. 6, pp. 1217–1228, Dec. 2003.

[27] P. Rodriguez, "Current-force- and vibration based techniques for induction motor condition monitoring," Ph.D. dissertation, Helsinki Univ. Technol., Espoo, Finland, 2007.

[28] T. K. Sarkar, M. Salazar-Palma, and M. C. Wicks, *Wavelet Applications in Engineering Electromagnetics*. Norwood, MA: Artech House, 2002.

[29] M. V. Mickerhauser, *Adapted Wavelet Analysis From Theory to Software*. Natick, MA: Wellesley, 1994.

[30] A. N. Akansu and R. A. Haddad, *Multi-Resolution Signal Decomposition Transforms, Sub-bands, and Wavelets*, 2nd ed. New York: Academic, 2001.

[31] M. Misiti, Y. Misiti, G. Oppenheim, and J. M. Poggi, *Wavelet Toolbox, User's Guide for Matlab*. Natick, MA: MathWorks, Jun. 2004.

[32] J. Cusido, A. Jornet, L. Romeral, J. A. Ortega, and A. Garcia, "Wavelet and PSD as a fault detection techniques," in *Proc. IEEE IMTC*, 2006, pp. 1397–1400.